Thermally-induced flexible and thermally conductive enhanced phase change material with 1-hexadecanol as phase change component

Lei Chen[a], Ruiqi Zhang[b], Xing Cao[b,*], Xuebing Li[a], Yongtao Qu[c]

[a]*Key Laboratory of Biofuels, Qingdao Institute of Bioenergy and Bioprocess Technology, Chinese Academy of Sciences, Qingdao 266101, China*

[b]*College of Electromechanical Engineering, Qingdao University of Science and Technology, Qingdao 266061, China*

[c]*Department of Mathematics, Physics and Electrical Engineering, Northumbria University, Newcastle upon Tyne, NE1 8ST, United Kingdom*

ABSTRACT

High latent heat and thermostatic properties of phase change materials (PCMs) have made them the promising materials. Herein, a novel thermally-induced flexible 1-Hexadecanol/Olefin block copolymer/Hexagonal boron nitride (HD/OBC/h-BN) composite phase change material (CPCM) is proposed. Bio-based non-polluting material of HD is employed innovatively as the phase change component. The triggering of HD phase transition can achieve various deformation modes for CPCM, which is beneficial to reduce the thermal contact resistance between CPCM and device. The electrically insulating property of h-BN not only improves the thermal conductivity and the heating/cooling rate of CPCM, but also further solves the problem of the HD leakage (as low as 0.31 wt%). The prepared CPCM with excellent flexibility and high latent heat (above 150 J/g) has good thermal stability and thermal reliability in the working temperature range. This provides developed CPCM greater potential for thermal energy storage (TES) and thermal management (TM) than conventional PCMs.

Keywords:

A. Energy materials

A. 3-Dimensional reinforcement

B. Thermal properties

Thermally-induced flexibility

---

*Corresponding author.

E-mail addresses: caoxing@qust.edu.cn (X. Cao).

1.Introduction

In recent years, the exploration of new technologies to achieve more efficient and cleaner ways to use and manage thermal energy has been a hot issue in the scientific community. Thermal energy utilization, such as solar heating [1, 2] and waste heat recovery [3, 4] relies on an efficient and economical thermal storage technology called thermal energy storage (TES), including sensible heat thermal energy storage and latent heat thermal energy storage (LHTES). LHTES uses a medium material with high latent heat to store surplus thermal energy and release the energy when needed. Its energy storage density is 5-14 times higher than that of sensible heat thermal energy storage, thus proves to be one of the powerful approaches for efficient energy storage and conversion [5-7]. Among a wide range of thermal management (TM) applications, including cooling of electronic components [8], building thermal management [9-11] and battery thermal management (BTM) [12-14] have received increasing attention in recent years. Recently, lithium-ion battery has been widely used in new energy fields such as electric and hybrid electric vehicles due to its high energy density, low cost and little memory effect [15]. However, lithium-ion battery has been proved to be very sensitive to temperature, which will significantly affect their capacity and power [16]. Therefore, it is crucial to construct an efficient BTM system to maintain the operating temperature of the

45 battery within the desired range. A large number of researchers have developed efficient BTM systems,
46 which can be mainly classified into two forms: active and passive. The former includes air and liquid
47 cooling, which usually requires additional equipment, energy consumption and space, while the latter form
48 achieves efficient thermal management without consuming external energy. It is therefore an extremely
49 promising technology for thermal management [17]. BTM system based on mediums with high latent heat
50 can effectively reduce the maximum temperature rise of batteries, and has excellent thermal management
51 characteristics.

52 As mentioned earlier, a medium is required in both TES and TM. It is called phase change material
53 (PCM), which is a substance that can absorb or release a large amount of latent heat at an approximately
54 constant temperature during the phase transition process. PCM-based TES and TM systems have
55 advantages of high thermal storage and thermal management capability without any additional power
56 consumption. PCM includes organic type (e.g. paraffin, fatty acids and fatty alcohols) and inorganic type
57 (e.g. salts, hydrated salts, metals and their alloys). The dominance of the organic type over the inorganic
58 type is the absence of disadvantages such as phase separation. Meanwhile, its degree of overcooling is much
59 lower than that of inorganic type. For the organic type, the fatty alcohol can be obtained from environmental
60 friendly renewable biological resources. Moreover, it has good thermal and chemical stability, high latent
61 heat storage capacity and suitable phase transition temperature. Compared to paraffin (PA) derived from
62 petroleum, fatty alcohols are low-cost, non-toxic and non-corrosive with low overcooling and no phase
63 separation [18]. It is worth noting that hexadecanol (HD) has a suitable phase transition temperature and
64 high enthalpy as well as a good compatibility with other components of the composites.

65 Although fatty alcohols have many advantages, the tendency to leak after melting has obviously limited
66 its application in TES and TM applications [19, 20]. Polymeric materials or porous materials are usually

added as supporting matrix to prepare shape-stabilized composite PCM (CPCM) to limit the leakage of liquid PCM. Literatures are devoted to high-density polyethylene (HDPE) [21], low density polyethylene (LDPE) [22], polystyrene (PS) [23], polymethyl methacrylate (PMMA) [24], epoxy resin (ER) [25] and expanded graphite (EG) [26] as the supporting matrix of PCMs. Furthermore, Li et al. [27] employed cellulase hydrolyzed wood as the supporting material and used polyethylene glycol (PEG) as the PCM component. The prepared CPCMs have good mechanical properties, high energy storage capacity (151.74 J/g), anisotropic thermal conductivity and good thermal stability. Trigui et al. [28] prepared the shape-stabilized PCM based on LDPE using physical melting and mixing method. The results showed that the LDPE matrix could maintain the shape of the composite at the macroscopic level during the phase transition of PA. Wang et al. [29] focused on a novel shape-stabilized phase change material which was prepared by wrapping PA in ER. The results showed that the prepared material has good thermal reliability and leakage-proof performance. The mass loss of CPCM was only 0.349 wt% after 100 thermal cycles, which effectively prevented the leakage of PA. Jiang et al. [30] fabricated the PA/EG CPCM for BTM applications. The results showed that the leakage rate of PA decreased with the increase of EG content. For the CPCM sample containing 30 wt% EG, the leakage rate was only 0.38%. Liu et al. [26] used expanded perlite (EP) as the supporting material. The PCMs were capric acid and myristic acid with a mass ratio of 9:1, which were mixed into cement mortar to prepare a novel building envelope to improve the thermal comfort of the building. The experimental results showed that the prepared materials have good thermal stability and leakage-proof performance.

Most of the above research have focused on overcoming the problem of leakage to prepare shape-stabilized CPCMs. However, assembly issues must be considered when designing some specific systems, such as PCM-based BTM systems. Conventional CPCMs have high rigidity, which can lead to low ease of

89 installation between the device (e.g. cylindrical lithium-ion battery) surface and the CPCM, high thermal
90 contact resistance and energy dissipation [1]. Therefore, functionalizing the CPCM to overcome the above-
91 mentioned defects is a promising research direction. In recent years, some novel materials, such as flexible
92 nanoporous boron nitride aerogel [31], olefin block copolymer (OBC) [32], polydimethylsiloxane (PDMS)
93 [33], polyolefin elastomers (POE) [9], Styrene-butadiene-styrene (SBS) [34], melamine foam (MF) [8] and
94 other elastic polymers have received a lot of attention in the preparation of flexible phase change materials.
95 Yang et al. [9] developed CPCM flexible film based on POE and styrene-b-(ethylene-co-butylene)-b-
96 styrene triblock copolymer (SEBS) by a novel cross-linked polymer swelling strategy. The experimental
97 results illustrate that the film can reduce the temperature of electronic device and building by 5.5°C and
98 9.3°C, respectively. This demonstrates a great potential for thermal management applications. Wu et al. [35]
99 successfully prepared a novel shape-stabilized thermally-induced flexible CPCM with PA as PCM and OBC
100 as supporting material. The good flexibility of this material is achieved by triggering the phase transition
101 of PA, which is beneficial to reduce the thermal contact resistance. Xiao et al. [8] employed a flexible
102 CPCM using copper-coated melamine foam (MF@Cu) as the supporting material and polyethylene glycol
103 (PEG) as the phase change component, which can be applied to the thermal management of electronic
104 device. Huang et al. [36] successfully prepared a novel flexible composite SBS@PA/EG by using PA as the
105 phase change component and SBS as the supporting material. This CPCM was successfully applied in BTM
106 system. Among various elastic polymers, OBC has potential applications in TES and TM. OBC is
107 commonly used as a supporting material for PA, while little research has been performed on CPCM using
108 other PCMs (i.e., non-PA) as phase change components. Research in this direction is important for
109 expanding the application of this type of elastic material and the realization of energy saving and
110 environmental protection.

111 Thermal performance includes thermal conductivity, thermal convection, thermal stability and many
112 other aspects. For CPCM, the demonstration of thermal performance is often the result of a combination of
113 factors. Among them, thermal conductivity is a very important factor in thermal performance. Improving
114 the thermal conductivities of shape-stabilized CPCMs with polymers as supporting materials remains a
115 great challenge [37, 38]. The thermal conductivity of organic PCMs (e.g. paraffin, fatty acids and fatty
116 alcohols) is approximately 0.2 $W \cdot m^{-1} \cdot K^{-1}$, while the thermal conductivity of polymers is similar. The low
117 thermal conductivity of CPCM is likely to cause a considerable temperature gradient inside CPCM during
118 heat absorption and release, resulting in a large accumulation of heat in concentrated areas and thus causing
119 the phenomenon of thermal runaway. In order to solve this problem, the researchers have conducted
120 numerous experimental studies on high thermal conductivity fillers such as metal foam [39], metal oxides
121 [40], EG [32], carbon nanotubes [41], carbon fiber [42], BN [43], etc. Li et al. [44] constructed hybrid
122 supporting materials using porous cellulose nanofibril (CNF) and silver nanowire (AgNW) through a
123 directional freeze-drying method to encapsulate octadecanol (OCO) and octodecane (OCC). The obtained
124 series of CPCMs showed improved thermal conductivity, good thermal stability and thermal reliability,
125 which can be employed for renewable thermal energy storage systems. Wu et al. [1] used graphene oxide
126 (RGO) as a thermal conductivity filler to prepare a shape-stabilized PA/MF/RGO CPCM with solar-to-
127 thermal energy storage ability. This can be utilized in the field of solar energy utilization and energy-saving
128 buildings. Döğüşcü et al. [45] used HD as the PCM, polystyrene as the supporting matrix, and carbon
129 nanofibers as thermal conductivity fillers to prepare the form-stable PCMs. The thermal conductivity of
130 prepared CPCM is higher than that of pure PCM. The results show that the higher content of carbon
131 nanofibers result in the higher thermal conductivity of CPCM. When the mass fraction of carbon nanofibers
132 is 1.0 wt%, the thermal conductivity of CPCMs is 0.175 $W \cdot m^{-1} \cdot k^{-1}$. Zhang et al. [46] prepared a flexible

PCM based on silicone rubber (SR) using BN as thermal conductivity fillers. This CPCM provided both battery thermal management and anti-collision performance with a thermal conductivity of up to 0.95 $W \cdot m^{-1} \cdot k^{-1}$, which is 5.28 times and 4.52 times higher than that of pure SR and pure PA, respectively. Among various thermal conductivity fillers, h-BN, with a structure similar to graphite has excellent thermal and chemical stability. Because of its high thermal conductivity (33 $W \cdot m^{-1} \cdot K^{-1}$) and electrical insulating property, it is extremely suitable to be used as the thermal conductivity filler in TES and TM. However, most of the studies are only limited to its effect on the overall thermal conductivity enhancement magnitude, and lacked of better mathematical model analysis. A combination of theoretical and experimental values would help to provide a comprehensive understanding of the h-BN. The exploration of this thermal conductivity filler is therefore of great importance.

Considering all mentioned challenges above, a novel h-BN enhanced flexible HD/OBC/h-BN CPCM has been successfully prepared in this paper. OBC is used as the supporting matrix, which solves the leakage of HD and endows the thermal-induced flexibility. As the thermal conductivity filler, h-BN improves the thermal conductivity of CPCM. The effect of OBC and h-BN on thermal conductivity, phase change performance, leakage and sensitive flexibility and thermal and cycle stability are discussed carefully. The crystalline structure, morphology structure, and thermal properties are tested by X-ray diffraction (XRD), scanning electron microscope (SEM), differential scanning calorimetry (DSC) and thermal gravimetric analysis (TGA). Furthermore, the heat transfer performance of the samples is tested experimentally. The prepared shape stabilized CPCM sample exhibits excellent thermal properties and good flexibility, which can be applied to TES and TM applications.

2. Experimental section

2.1. Materials

1-Hexadecanol (HD, AR, Sinopharm Chemical Reagent Co., Ltd, China) with a melting point of 58.7 °C was selected as phase change component because of its suitable melting point and high latent heat (about 220 J/g). OBC (Model 9530, Dow Chemical Company, USA) with a density of 0.887 $g \cdot cm^{-3}$ and a melt flow rate of 5 g/10 min (190 °C/2.16 kg) was used as the supporting material for the CPCMs. The h-BN powder (99.9% purity, Aladdin Reagent, China) with an average size of 1~2 μm was used as the thermal conductive and insulation filler. All chemicals were used directly without any treatment.

2.2. Preparation

In this paper, a series of the HD/OBC CPCMs modified by different content of h-BN powder were prepared through the physical melting and mixing method, as illustrated in Fig. 1. And the component proportion of CPCMs is shown in Table 1. To avoid the error caused by mass difference, the total quality of each sample was 20 g. Firstly, the pure HD and OBC were weighed using an electronic balance and mixed in a beaker. The mixture was stirred in an oil bath at 160 °C for 30 min at 1200 rpm until completely melting to yield a homogeneous solution of HD/OBC. Secondly, certain content of h-BN powder was added into the HD/OBC solution and mixed with continuous stirring at 160 °C for 30 min at 1200 rpm to obtain HD/OBC/h-BN CPCM. Ultimately, prepared mixtures (i.e., HD/OBC, HD/OBC/h-BN) were poured into a mold with the size of 25 mm in diameter for hot-pressing and then cooled for 24 hours at room temperature to obtain the compressed samples. The as-prepared samples were polished to form round thin cakes with smooth surface. The prepared samples placed in beakers can be seen in Fig. 1.

2.3. Characterization

2.3.1. Chemical characterization

X-ray diffractometer (XRD, D8, Germany) with a scanning rate of 5° (2θ) min^{-1} and a scanning range of 5-80° was used to determine the chemical characterization of the composites.

177 **2.3.2. Microstructure and morphology characteristics**

178 The microstructure and morphology of h-BN and CPCM were investigated by a scanning electron
179 microscope (SEM, S4800, Japan) with 5 kV working voltage. In order to avoid unclear photographs due to
180 low electronic conductivity, all samples were treated with gold spray.

181 **2.3.3. Thermal properties**

182 The DSC analysis for thermal properties of the samples including extrapolation peak onset temperature,
183 melting peak temperature and enthalpy were determined using a simultaneous thermal analyzer (STA, HCT-
184 1, China) in nitrogen atmosphere at 100 mL · min^{-1} flow speed. Each sample ranged from 7 mg to 13 mg
185 was accurately weighed with an electronic balance and sealed in the center of crucible made of aluminium
186 oxide. The phase transition curve was obtained at the temperature rising speed of 10 °C · min^{-1} and the
187 operating temperature range of 25 °C-100 °C. The TGA for thermal stability was tested by a simultaneous
188 thermal analyzer (STA, HCT-1, China) with the operating temperature range of 25 °C-600 °C at the rate of
189 10 °C · min^{-1} in the nitrogen atmosphere. Based on the transient hot-wire method, the thermal conductivity
190 was obtained by thermal conductivity instrument (TC3000D, China) with precision of ±3%. The instrument
191 was pre-heated for 30 min before measurement. The experimental voltage during measurement was 1 V.
192 The data acquisition was performed every 3 min with the acquisition process lasting 2 s and repeated 10
193 times at room temperature. The CPCM was produced into two cakes of 50 mm diameter and 10 mm
194 thickness, which was polished with sandpaper. The measurement is then carried out by sandwiching the
195 test sensor between the samples, ensuring that the hot wire is completely covered by the samples.

196 **2.3.4. Form-stable ability and thermal reliability**

197 The form-stable ability of compressed CPCM samples was analyzed via leakage test. Each sample
198 with initial mass M_0 was placed in beaker respectively. The samples were placed into vacuum drying oven

199 at 70°C. After 30 min, taking out the samples and weighing them by electronic balance. Then, the beaker
200 was cleaned and dried before putting samples back in the vacuum drying oven. The mass of samples for n-
201 times is recorded as M_n. L_n is the leakage rate at the n-times. The leakage rate was calculated as following
202 (i.e., Eq. 1):

203 $$L_n = \frac{M_0 - M_n}{M_0} \times 100\% \quad (1)$$

204 The high-low temperature alternating test chamber was used for thermal cycling operations to determine
205 the thermal reliability of CPCM. The operating temperature range was set from 25 °C to 70 °C at the rate
206 of 10 °C · min^{-1}. The constant temperature of 5 min was set after reaching the set temperature to ensure that
207 the samples had been completely phase transition. After 200 cycles, the DSC and SEM measurements were
208 conducted.

209 **2.3.5. Heat transfer characterization**

210 The heat transfer performance of the pure HD and CPCM was investigated by heat storage and release
211 experiment. The test system consisted of Agilent data acquisition module (Agilent 34970A, USA),
212 computer terminal and thermostatic oil bath (DF-101S, China), as shown in Fig. 2. After weighing 20 g of
213 pure HD and CPCM in 50 mL beakers, the samples were placed in the thermostatic oil bath to melt
214 completely. The samples were cooled to room temperature after inserting K-type thermocouples into the
215 middle of them. In addition, the temperature of the experimental environment (T_a) was recorded with
216 another thermocouple. The temperature of oil bath was set to 70 °C and each sample was thermally
217 equilibrated at 25°C for a period. Then, the samples were placed in the oil bath. When the temperature of
218 samples no longer fluctuates, the samples were removed from the oil bath and placed in the air to cool to
219 25 °C. Finally, the temperature curves were obtained from the heating and cooling processes.

220 **3. Results and Discussion**

3.1. Crystalline structure and morphology

The chemical compatibility of the components in CPCM was analyzed by XRD, as shown in Fig. 3. For pure HD, the sharp diffraction peaks appearing at 21.72° and 24.61° represent the crystallization of HD, which is attributed to the diffraction of (-6 1 1) and (14 0 2) crystal planes. The diffraction peaks of OBC are captured at 13.96° and 16.71°. The XRD pattern of S4 contains all the peaks of HD and OBC. In the XRD pattern of h-BN, a strong diffraction peak is observed near 26.66°, which is corresponding to the feature peak (0 0 2) of BN. Since S7 of HD/OBC/h-BN composite is composed of S4 HD/OBC and h-BN particles, it can be seen that the range of peaks appearing in S7 correspond well to the diffraction peaks of S4 and h-BN. No new peaks can be observed in S7, indicating that the HD/OBC/h-BN composites are physical mixes and there is no change in the crystalline form. It is further found that the diffraction peak intensity of S7 at 26.66° is relatively lower in comparison with that of pure h-BN, which is due to the low loading of h-BN in S7.

Morphology structural characterization of h-BN, HD/OBC (S4) and HD/OBC/h-BN (S7) composites are presented in Fig. 4. As shown in Fig. 4(a) and Fig. 4(d), it can be seen that h-BN is tiny particle with the size of 1~2 μm. Such tiny particles provide a high specific surface area. As displayed in Fig. 4(b) and Fig. 4(e), the morphology of HD/OBC shows a laminar structure with no indication of immiscibility between HD and OBC, indicating that HD can be dispersed well into the OBC network [47]. In addition, the three-dimensional network structure of the OBC facilitates the adsorption of HD, which is essential for the shape stability of CPCM. As shown in Fig. 4(c) and Fig. 4(f), the poor compatibility between h-BN and HD/OBC makes h-BN easily distinguished in CPCM. The h-BN is distributed in the whole vision and still maintains a particle size of 1~2 μm without agglomeration. The reason is that the porosity structure of HD/OBC can absorb h-BN particles and prevent them from agglomeration and settlement. Meanwhile, h-

BN with the high specific surface area distributed on the OBC can fix HD to a certain extent, further enhancing the shape stability and thermal conductivity of CPCM.

3.2. Thermal conductivity enhancement

Thermal conductivity is an important property because it is closely related to thermal performance in various practical applications. As mentioned before, HD and OBC are organic materials with low thermal conductivity and so are their blends. In this work, h-BN with different mass fractions was added into the HD/OBC blends to enhance the thermal conductivity. Fig. 5 indicates the thermal conductivity of samples with different h-BN mass fractions at room temperature. Fig. S1 and Table S1 show the specific data, average, standard deviation and CV% of 10 measurements. It can be seen that the overall thermal conductivity increases almost linearly with the mass fraction of h-BN. The h-BN with high specific surface area can effectively increase the thermal conductivity. The results showed that the thermal conductivity of HD/OBC/h-BN composites is 0.26965 $W \cdot m^{-1} \cdot k^{-1}$, 0.28350 $W \cdot m^{-1} \cdot k^{-1}$ and 0.30225 $W \cdot m^{-1} \cdot k^{-1}$ when the mass fraction of h-BN is 1 wt%, 5 wt% and 10 wt% respectively, which is 3.83%, 9.16% and 16.38% higher than that of the HD/OBC blend (0.25970 $W \cdot m^{-1} \cdot k^{-1}$).

In general, the effective thermal conductivity of CPCMs is strongly influenced by their composition. Many analytical models have been proposed for the thermal conductivity of composites such as the classical Maxwell-Eucken model. In this work, the Maxwell-Eucken model, as shown in Eq. 2, was used to investigate the effective thermal conductivity of HD/OBC/h-BN composites.

$$k_e = k_{HD/OBC} \frac{2k_{HD/OBC} + k_{BN} - 2(k_{HD/OBC} - k_{BN})(1 - v_{HD/OBC})}{2k_{HD/OBC} + k_{BN} + (k_{HD/OBC} - k_{BN})(1 - v_{HD/OBC})} \quad (2)$$

The Maxwell-Eucken model is a classical model well suited for estimating the thermal conductivity of porous composites based on the rule of mixture of composite, which represents the homogeneous dispersion of one medium in another medium with disconnected pores in the dispersed phase, resulting in a composite

containing two components. Meanwhile, Maxwell-Eucken model does not take the effect of the composite's bulk density into account [48]. In order to deal with the mathematical model of the HD/OBC/h-BN ternary material, the HD/OBC blend was treated as a single component with equivalent physical properties. Its density was experimentally tested to be 0.92280 g/cm^3 and the thermal conductivity was tested to be 0.25970 $W \cdot m^{-1} \cdot k^{-1}$. The comparison of the measured values with the predicted values shows in Fig. 5. The measured thermal conductivity of S6 is 0.26965 $W \cdot m^{-1} \cdot k^{-1}$, while the predicted value is 0.26280 W $\cdot m^{-1} \cdot k^{-1}$; the measured value of S7 and S8 is 0.28350 $W \cdot m^{-1} \cdot k^{-1}$ and 0.30225 $W \cdot m^{-1} \cdot k^{-1}$, while the predicted value is 0.27590 $W \cdot m^{-1} \cdot k^{-1}$ and 0.29410 $W \cdot m^{-1} \cdot k^{-1}$ respectively. The maximum deviation between measured and predicted values is only 2.7%. Therefore, the mathematical model of the HD/OBC/h-BN ternary composite can be reasonably predicted theoretically by the Maxwell-Eucken model. However, it is worth noting that the deviation of predicted value and CV% of measurements are gradually increasing with the increase of h-BN addition. This is due to the fact that as the amount of h-BN added increases, the performance impact of its uneven dispersion will be more significant. Meanwhile, it can be demonstrated that the samples prepared in this work are well mixed and the h-BN is well distributed as a dispersed phase in the HD/OBC continuous phase.

3.3. Phase change performance

The phase transition property of PCM is essential. The DSC heating curves of pure HD and CPCMs are shown in Fig. 6 and the corresponding extrapolation peak onset temperature (T_e), melting peak temperature (T_m) and enthalpy (ΔH_m) are listed in Table 2. The phase transition temperature mentioned in this paper refers to the melting peak temperature. As shown in Fig. 6(a) and Table 2, the melting peak temperatures of S1-S5 change slightly compared to that of HD with a maximum variation of only 4.77%, which shows the effect of OBC on the phase transition temperature of HD is minimal. The enthalpy of pure HD is 0.22

kJ/g. As content of OBC increases from 10 wt% to 50 wt%, enthalpy of the HD/OBC blends is found to decrease. The lowest value is 0.14 kJ/g for S5, demonstrating that OBC cannot provide the latent heat storage capacity in the experimental temperature range. To further investigate the effect of h-BN on the phase transition property of CPCM, DSC test was done on S6, S7 and S8. The heating curves are shown in Fig. 6(b) with melting peak temperature of 61.2 °C, 61.6 °C and 57.4 °C for S6, S7 and S8, respectively. Compared with S4, the maximum change is only 3.69%. The results show that h-BN has little effect on the phase transition temperature of HD/OBC. The enthalpy fluctuates only slightly with the addition of 1 wt%, 5 wt% and 10 wt% h-BN powder, respectively. Since h-BN also does not have the ability to store latent heat, the effect of adding 1 wt% of h-BN on the enthalpy is almost negligible from the experimental results. The addition of 5 wt% and 10 wt% h-BN leads to a corresponding decrease in enthalpy, but still remains in a high level.

3.4. Leakage and sensitive flexibility experiment

Pure HD exhibits the strong rigidity and fragility when subjected to external forces at room temperature of 25°C, as shown in Fig. 7(a-b). This can lead to problems with installation and integration, resulting in high interface thermal contact resistance between the PCM and controlled device and affecting overall performance. Furthermore, as shown in Fig. 7(c-d), HD melts completely to the pure liquid state when experimental temperature is higher than the phase transition temperature of HD. For organic PCMs, the solid-liquid phase transition not only raises leakage safety issues, but also affects their cycle reliability. Leakage test with thermal cycles between 25 °C and 70 °C was done to investigate the leakage-proof performance of prepared CPCMs. The results are shown in Fig. 8 and the photographs of each sample are listed in Table S2. The component of the leakage is mainly HD. As shown in Fig. 8(a), the leakage rate of S1 (with 10 wt% OBC) increased with the number of thermal cycles and reached 34.70% after 10 thermal

cycles. The leakage of HD is clearly visible in the beaker and the original shape of the sample is changed, indicating that 10 wt% OBC was not sufficient to restrict the leakage of HD and the shape stability of CPCM was poor. S2 (with 20 wt% OBC), S3 (with 30 wt% OBC), S4 (with 40 wt% OBC) and S5 (with 50 wt% OBC) have the leakage rate of 19.89%, 11.14%, 2.69% and 0.81% after 10 thermal cycles, respectively. The leakage rate decreases significantly with increasing the content of OBC in HD/OBC. The three-dimensional network structure of OBC can wrap around the HD more effectively and restrict the flow of liquid HD to some extent [49]. Although S5 has the best shape stability, its latent heat of phase change (0.14 kJ/g) is inferior to that of S4 (0.16 kJ/g). Considering the shape stability and the latent heat of phase change, S6, S7 and S8 are all further added with h-BN through the S4 matrix. As shown in Fig. 8(b), the leakage rate of S6, S7 and S8 after 10 thermal cycles is 0.77%, 0.31% and 0.89%, respectively. Due to the leakage of HD, the reduction of HD proportion allows the h-BN to be better covered by the three-dimensional network structure of OBC, thus limiting the leakage of liquid HD to some extent [49]. It can be noted that the sample with 10 wt.% h-BN added (S8) had a higher leakage rate than the other samples. Due to the strong interaction between the h-BN particles, agglomeration is more likely to occur when too many particles are added. It can result in non-uniform dispersion of the h-BN, which further prevents it from being effectively covered by the three-dimensional network structure of the OBC. Therefore, adding the appropriate amount of h-BN can further reduce the leakage rate of CPCM. It is worth noting that sample S7, a CPCM based on S4 with the addition of 5 wt% h-BN, has an even lower leakage rate (0.31%) than that of S5 (0.81%) by 61.73%, while the enthalpy of S7 (0.15 kJ/g) is higher than that of S5 (0.14 kJ/g). In the prepared HD/OBC/h-BN CPCMs (i.e., S6, S7 and S8), the leakage rates after 10 thermal cycles are all less than 1 wt%, proving that CPCMs prepared in this paper have good leakage-proof capability.

Fig. 9 shows the basic mechanism of the shape-stabilized CPCM based on OBC and the form in which

it can withstand external forces. OBC as a thermoplastic polyolefin elastomer, is composed of crystallizable hard block and amorphous soft block. The hard block gives the OBC a high melting temperature and the soft block gives the OBC a low glass transition temperature. Based on the unique phase separation structure of OBC, the solid-liquid phase transition of HD can be used to enable the conversion between rigid and flexible CPCMs [49]. As a result, the CPCM is rigid at room temperature due to the solid HD, while the soft block of OBC prevents the liquid HD from leaking at high temperature and allows the CPCM to exhibit good flexibility under stretching, compression and torsion. To illustrate the thermal-induced flexibility of the prepared CPCM, S4 and S7 were heated in a vacuum drying oven at 70°C for 30 min. When thermal equilibrium is reached, HD is completely melted and the flexibility of S4 is triggered by the solid-liquid phase transition of HD. Therefore, the CPCM could be stretched/compressed/bent under external forces. For the sample filled with h-BN, the same rigid-flexible transition is exhibited under thermal trigger, as shown in Fig. 10. Each sample can be bent into any angle by external force. The pure HD subjected to external forces and the deformation modes of the prepared S4 and S7 are shown in Video S1, Video S2 and Video S3. The diversity of deformation modes allows the CPCM to be used in a variety of applications. The results show that the prepared CPCM can transform from a rigid material to a flexible material under thermal trigger, while h-BN has no effect on its rigidity-flexibility transformation properties.

3.5. Thermal and cycle stability

To analyze the thermal stability of CPCM at high temperature conditions, TGA tests were carried out. Fig. 11 shows the TGA curves of HD, OBC, HD/OBC (i.e., S1-S5) and HD/OBC/h-BN (i.e., S6-S8). From Fig. 11(a), it can be seen that both HD and OBC are one-step degradation with only one plateau during the decomposition process. The decomposition of HD begins at 161.7 °C and decomposes completely at 258.8 °C. OBC does not show obvious decomposition until 383.8 °C and decomposes completely at

464.9°C. For S1-S5, the TGA curves are divided into two processes. The first process from 160 °C to 300 °C is the decomposition of HD. The second process above 400 °C is the decomposition of OBC. The complete decomposition temperature reaches 481.3 °C (S5), which is an increase of 85.97% compared to that of HD (258.8 °C). As can be seen from Fig. 11(b), for S6-S8, the TGA curves are still divided into two processes. As the operating temperature increasing to 600 °C, some remaining residue can be found and is believed to be undecomposed h-BN as the mass content of residue is consistent with the loading ratio of h-BN in the PA/OBC/h-BN composites (S6-S8). For S8 (with 10 wt% h-BN), the temperature to reach 90 wt% mass loss is 517.9 °C, an increase of 100.12% and 13.08% relative to the complete decomposition temperature of HD and S4, respectively. It demonstrates that HD, OBC and h-BN can be mixed very successfully and the prepared CPCM has good thermal stability.

The thermal cycle stability of CPCM is a key point for practical engineering applications in TES and TM. The DSC curves measured for S7 before and after 200 thermal cycles are shown in Fig. 12. It can be seen that only a small shift can be observed after thermal cycles between 25-70 °C, indicating that the phase transition temperature of CPCM is not significantly affected by thermal cycling. In addition, the enthalpy of CPCM does not change obviously before and after thermal cycling and still maintains a high level of 0.15 kJ/g. Meanwhile, the SEM image of S7 after 200 thermal cycles is shown in the Fig. 13. A well-dispersed state of h-BN (marked by red circles) can be easily observed, which indicated that the phase transition occurring during thermal cycling does not cause significant changes in the h-BN dispersion. Therefore, the prepared CPCM after 200 thermal cycles has good thermal reliability.

3.6. Heat transfer performance

To further explore the effects of OBC and h-BN on the thermal performance of CPCM, the heat transfer characteristics of different samples were investigated. It can be seen from Fig. 14 that the ideal thermal

storage and release process can be divided into three stages, namely the heating stage (1-3), the thermal equilibrium stage (4) and the cooling stage (5-7), while there are seven specific stages contained within the three stages. The numerical symbols corresponding to the stages have been marked in Fig. 14.

The shape of transient temperature variation curves obtained through experiment of the samples in Fig. 15 (a) are similar to that of Fig. 14. In stage 1, phase transition of materials has not begun (i.e., remaining solid phase). The heat from the surrounding environment is absorbed by the samples in the form of sensible heat through the way of heat conduction between the samples and the surrounding environment. As can be seen in Fig. 15 (a), due to the difference in thermal conductivity, the temperature rising slope of the samples shows a significant variability. S7 has the highest thermal conductivity, followed by S4 and HD in that order. It is clear from Fig. 15(a) that the green line (S7) has the greatest slope, followed by the blue line (S4) and the red line (HD). When the temperature reaches the melting point of PCM, the temperature changing gradually slows down and a distinct plateau in temperature appears at stage 2, while the PCM begins to absorb heat in the form of latent heat. It is easy to distinguish from Fig. 15 that pure HD has the narrowest range of stage 2 of all samples (i.e., pure HD is the first to complete the phase transition process to end stage 2). This is due to the buoyancy force generated by the natural convection of liquid HD during the melting process, which enhances the heat transfer within the HD [17, 50]. While S4 and S7 are solid-state in macroscopic due to the limitation of the three-dimensional network structure of OBC, the natural convection of the internal melted HD is limited. Therefore, the heat transfer of S4 and S7 is low and the phase transition rate is slowed down. It is worth noting that the heat transfer efficiency of S7 is higher than S4 due to the higher thermal conductivity of S7 than S4. In Fig. 15(a), it is clear that the green line (S7) is the first to complete the phase transition process relative to the blue line (S4). It can also be noted that even though S7 has a relatively high thermal conductivity, its phase transition range is still longer than that of

HD. This is due to the fact that although HD has the lowest thermal conductivity, the promotion of heat transfer within the HD by the natural convection is more effective than increased thermal conductivity by h-BN. It greatly improves the heat transfer efficiency of the HD and completes the phase transition process prior to the S7. When the phase transition (i.e., stage 2) is complete, the heat is absorbed by the PCM in the form of sensible heat in stage 3, which implies an increase in temperature. In stage 4, the temperatures of samples all keep relatively constant as they reach the temperature close to the set point. During this stage, two phenomena can be observed. Firstly, the temperature of the environment and the thermal equilibrium temperature of the pure HD always fluctuate around 70 °C, which is due to the thermostatic mode of the oil bath. While for S4 and S7, there is no temperature fluctuation, indicating that the CPCM has good thermostatic characteristics. Secondly, the environment temperature is set at 70 °C and the thermal equilibrium temperature of pure HD also reached 70 °C, while S4 and S7 both reached a maximum temperature of 63 °C. This is the effect of the OBC-based CPCM on the control of the maximum temperature rise [51], which has a good effect on the temperature control of the battery surface in BTM applications. The transient temperature curves of the cooling process are similar to that of the heating process. It is noteworthy that in stage 6, the S7 with the highest thermal conductivity, completes the phase transition first, followed in turn by S4 and HD. Different from the natural convection effect of HD during the heating process, the natural convection is suppressed by the high viscosity of the molten HD during cooling process, while the large enthalpy and low thermal conductivity further prolongs the freezing time [35]. Several papers give the same conclusions as this paper as to the reasons for the differences in the phase transition processes between the heating and cooling, such as [35], [49], [50] and [52].

$$\Delta T = T_a - T_n \tag{3}$$

To further analyze the effects of OBC and h-BN on the heat transfer performance of CPCM, the transient

419 temperature difference (ΔT) between sample and environment was introduced as shown in Eq. 3, where T_a
420 is the environment temperature, which was set to 70 °C in this paper. T_n is the sample temperature where n
421 contains HD, S4 and S7. Table 3 more accurately reflects the time spans required for the phase transition
422 of pure HD and CPCM during heating and cooling process in Fig. 15. As shown in Fig. 15(b), as previously
423 mentioned, the addition of OBC limits the natural convection of the molten HD and slows down the phase
424 transition during the heating process. As a result, the phase transition range of S4 is extended by 175%
425 compared to that of pure HD during the heating process. During the cooling process, the material releases
426 a large amount of latent heat stored in pure HD during the heating process, while OBC leads to lower latent
427 heat storage in CPCM. Therefore, compared to pure HD, the phase transition range of S4 is reduced by
428 64.27%. As the parts of the curves marked by enlargement in the Fig. 15(b), during the phase transition
429 process, it can be noted that the ΔT of S4 is smaller than that of pure HD, and the ΔT of S7 is smaller than
430 that of S4. As a result, the addition of h-BN leads to a reduction in ΔT during the phase transition process.
431 Meanwhile, excluding the effect of natural convection, the temperature of the sample will reach constant
432 more quickly. During the heating and cooling process, the phase transition range for S7 is reduced by 17.32%
433 and 21.71% compared to S4, respectively.

434 Therefore, it can be considered that the heating and cooling process are influenced by three main factors:
435 thermal conduction, natural convection and latent heat. It is worth noting that the prepared CPCM has two
436 advantageous features for practical engineering applications. Firstly, the phase transition range of stage 2
437 can be matched to the optimal battery operating temperature recommended in BTM. The purpose is to keep
438 the battery temperature near the recommended temperature range, thus improving electrochemical
439 performance, extending lifespan of battery and increasing efficiency. Secondly, the temperature difference
440 in stage 4 can alleviate thermal runaway of device to some extent, effectively reducing the maximum

441 temperature rise, increasing safety and effectively reducing economic losses.

442 **4. Conclusions**

443 Conventional organic PCMs play an important role in TES and TM because of their high latent heat
444 storage capacity and approximately constant temperature during the phase transition process. However,
445 their characteristics such as aggravating fossil energy consumption, easy leakage, low thermal conductivity,
446 rigidity and fragility limit their applications. Therefore, in this study, a novel environmentally friendly and
447 flexible HD/OBC/h-BN composite with a good shape stability is successfully fabricated. It is thermally
448 flexible and electrically insulating while solving the above problems. XRD and SEM characterization
449 showed the good physicochemical compatibility between the components of the composite. DSC and
450 leakage tests show that 40 wt% OBC can effectively prevent leakage of liquid-phase HD while maintaining
451 a high level of the latent heat. There are significant advantages in TES due to the high enthalpy of CPCMs.
452 The addition of h-BN can further reduce the leakage rate while improving the overall thermal conductivity
453 of CPCMs. The leakage rate of the CPCM with 5 wt% h-BN is only 0.31%. Based on the Maxwell-Eucken
454 model, the mathematical method of treating HD/OBC blend as a single component with equivalent physical
455 properties is validated, demonstrating that the method can better predict the thermal conductivity of this
456 type of ternary material. TGA and thermal cycling tests confirm the good thermal stability and thermal
457 reliability of CPCMs. In the heat transfer performance experiments, h-BN results in a shorter time to reach
458 a stable sample temperature, while the CPCM effectively reduces the maximum temperature rise and
459 suppresses temperature fluctuation, giving a clear advantage in TM. The prepared CPCM (with HD as PCM)
460 has a suitable phase transition temperature and high latent heat storage capacity. The thermally-induced
461 flexibility of CPCM can reduce its thermal contact resistance between the CPCM and device, and
462 effectively improve the efficiency. These advantages make this developed CPCM in this paper a great

potential for TES and TM applications that cannot be ignored.

Declaration of competing interest

The authors declare that they have no known competing financial interests or personal relationships that could have appeared to influence the work reported in this paper.

Acknowledgements

This work was supported by the Shandong Energy Institute (No. SEI-I202125), the Shandong Provincial Natural Science Foundation (No. ZR2018PEE017), the Application Foundation Research Program of Qingdao (No. 17-1-1-17-jch) and the National Natural Science Foundation of China (No. 21808235).

References

[1] Wu H-Y, Li S-T, Shao Y-W, Jin X-Z, Qi X-D, Yang J-H, et al. Melamine foam/reduced graphene oxide supported form-stable phase change materials with simultaneous shape memory property and light-to-thermal energy storage capability. Chem Eng J 2020; 379: 122373.

[2] Calle Adl, Bayon A, Pye J. Techno-economic assessment of a high-efficiency, low-cost solar-thermal power system with sodium receiver, phase-change material storage, and supercritical CO_2 recompression Brayton cycle. Sol Energy 2020; 199: 885-900.

[3] Chen D, Zhang R, Cao X, Chen L, Fan X. Numerical investigation on performance improvement of latent heat exchanger with sextant helical baffles. Int J Heat Mass Tran 2021; 178: 121606.

[4] Cao X, Zhang R, Chen D, Chen L, Du T, Yu H. Performance investigation and multi-objective optimization of helical baffle heat exchangers based on thermodynamic and economic analyses. Int J Heat Mass Tran 2021; 176: 121489.

[5] Jebasingh BE, Arasu AV. Characterisation and stability analysis of eutectic fatty acid as a low cost cold

energy storage phase change material. J Energy Storage 2020; 31: 101708.

[6] Veerakumar C, Sreekumar A. Phase change material based cold thermal energy storage: Materials, techniques and applications-A review. Int J Refrig 2016; 67: 271-289.

[7] Zhang R, Chen D, Chen L, Cao X, Li X, Qu Y. Preparation and thermal properties analysis of fatty acids/1-hexadecanol binary eutectic phase change materials reinforced with TiO_2 particles. J Energy Storage 2022; 51: 104546.

[8] Xiao Y-Y, Bai D-Y, Xie Z-P, Yang Z-Y, Yang J-H, Qi X-D, et al. Flexible copper foam-based phase change materials with good stiffness-toughness balance, electro-to-thermal conversion ability and shape memory function for intelligent thermal management. Compos Part A-Appl S 2021; 146: 106420.

[9] Yang L-Y, Feng C-P, Bai L, Bao R-Y, Liu Z-Y, Yang M-B, et al. Flexible shape-stabilized phase change materials with passive radiative cooling capability for thermal management. Chem Eng J 2021; 425: 131466.

[10] Huang J, Wu B, Lyu S, Li T, Han H, Li D, et al. Improving the thermal energy storage capability of diatom-based biomass/polyethylene glycol composites phase change materials by artificial culture methods. Sol Energ Mat Sol C 2021; 219:110797.

[11] Veerakumar C, Sreekumar A. Thermo-physical investigation and experimental discharge characteristics of lauryl alcohol as a potential phase change material for thermal management in buildings. Renew Energ 2020; 148: 492-503.

[12] Kolodziejczyk F, Mortazavi B, Rabczuk T, Zhuang X. Machine learning assisted multiscale modeling of composite phase change materials for Li-ion batteries' thermal management. Int J Heat Mass Tran 2021; 172: 121199.

[13] Liu Z, Huang J, Cao M, Jiang G, Yan Q, Hu J. Experimental study on the thermal management of

507 batteries based on the coupling of composite phase change materials and liquid cooling. Appl Therm
508 Eng 2021; 185: 116415.
509 [14] Galazutdinova Y, Ushak S, Farid M, Al-Hallaj S, Grágeda M. Development of the inorganic composite
510 phase change materials for passive thermal management of Li-ion batteries: Application. J Power
511 Sources 2021; 491: 229624.
512 [15] Akbarzadeh M, Jaguemont J, Kalogiannis T, Karimi D, He J, Jin L, et al. A novel liquid cooling plate
513 concept for thermal management of lithium-ion batteries in electric vehicles. Energ Convers Manage
514 2021; 231: 113862.
515 [16] Wu W, Wu W, Qiu X, Wang S. Low-temperature reversible capacity loss and aging mechanism in
516 lithium-ion batteries for different discharge profiles. Int J Energ Res 2019; 43: 243-253.
517 [17] Fan R, Zheng N, Sun Z. Evaluation of fin intensified phase change material systems for thermal
518 management of Li-ion battery modules. Int J Heat Mass Tran 2021; 166: 120753.
519 [18] Kenisarin MM. Thermophysical properties of some organic phase change materials for latent heat
520 storage. A review. Sol Energy 2014; 107: 553-575.
521 [19] Zhao Y, Min X, Huang Z, Liu Y, Wu X, Fang M. Honeycomb-like structured biological porous carbon
522 encapsulating PEG: A shape-stable phase change material with enhanced thermal conductivity for
523 thermal energy storage. Energ Buildings 2018; 158: 1049-1062.
524 [20] Min X, Fang M, Huang Z, Liu Y, Huang Y, Wen R, et al. Enhanced thermal properties of novel shape-
525 stabilized PEG composite phase change materials with radial mesoporous silica sphere for thermal
526 energy storage. Sci Rep-UK 2015; 5: 12964.
527 [21] Mu M, Basheer P, Sha W, Bai Y, McNally T. Shape stabilised phase change materials based on a high
528 melt viscosity HDPE and paraffin waxes. Appl Energ 2016; 162: 68-82.

529 [22] Lv Y, Liu G, Zhang G, Yang X. A novel thermal management structure using serpentine phase change
530 material coupled with forced air convection for cylindrical battery modules. J Power Sources 2020; 468:
531 228398.
532 [23] Fang Y, Yu H, Wan W, Gao X, Zhang Z. Preparation and thermal performance of polystyrene/n-
533 tetradecane composite nanoencapsulated cold energy storage phase change materials. Energ Convers
534 Manage 2013; 76: 430-436.
535 [24] Wang Y, Xia TD, Feng HX, Zhang H. Stearic acid/polymethylmethacrylate composite as form-stable
536 phase change materials for latent heat thermal energy storage. Renew Energ 2011; 36(6): 1814-1820.
537 [25] Mao D, Chen J, Ren L, Zhang K, Yuen MM, Zeng X, et al. Spherical core-shell Al@Al_2O_3 filled epoxy
538 resin composites as high-performance thermal interface materials. Compos Part A-Appl S 2019; 123:
539 260-269.
540 [26] Liu C, Luo C, Xu T, Lv P, Rao Z. Experimental study on the thermal performance of capric acid-
541 myristyl alcohol/expanded perlite composite phase change materials for thermal energy storage. Sol
542 Energy 2019; 191: 585-595.
543 [27] Li Y, Chen Y, Huang X, Jiang S, Wang G. Anisotropy-functionalized cellulose-based phase change
544 materials with reinforced solar-thermal energy conversion and storage capacity. Chem Eng J 2021; 415:
545 129086.
546 [28] Trigui A, Karkri M, Krupa I. Thermal conductivity and latent heat thermal energy storage properties
547 of LDPE/wax as a shape-stabilized composite phase change material. Energ Convers Manage 2014; 77:
548 586-596.
549 [29] Wang Z, Situ W, Li X, Zhang G, Huang Z, Yuan W, et al. Novel shape stabilized phase change material
550 based on epoxy matrix with ultrahigh cycle life for thermal energy storage. Appl Therm Eng 2017; 123:

1006-1012.

[30] Jiang G, Huang J, Fu Y, Cao M, Liu M. Thermal optimization of composite phase change material/expanded graphite for Li-ion battery thermal management. Appl Therm Eng 2016; 108: 1119-1125.

[31] Wang B, Li G, Xu L, Liao J, Zhang X. Nanoporous Boron Nitride Aerogel Film and Its Smart Composite with Phase Change Materials. Int J Energ Res 2020; 14: 16590-16599.

[32] Wu W, Liu J, Liu M, Rao Z, Deng H, Wang Q, et al. An innovative battery thermal management with thermally induced flexible phase change material. Energ Convers Manage 2020; 221: 113145.

[33] Shi Y, Hu M, Xing Y, Li Y. Temperature-dependent thermal and mechanical properties of flexible functional PDMS/paraffin composites. Mater Design 2020; 185: 108219.

[34] Huang Q, Deng J, Li X, Zhang G, Xu F. Experimental investigation on thermally induced aluminum nitride based flexible composite phase change material for battery thermal management. J Energy Storage 2020; 32: 101755.

[35] Wu W, Wu W, Wang S. Form-stable and thermally induced flexible composite phase change material for thermal energy storage and thermal management applications. Appl Energ 2019; 236: 10-21.

[36] Huang Q, Li X, Zhang G, Deng J, Wang C. Thermal management of Lithium-ion battery pack through the application of flexible form-stable composite phase change materials. Appl Therm Eng 2021; 183 (Part 1): 116151.

[37] Zhao Y, Sun B, Du P, Min X, Huang Z, Liu Y, et al. Hierarchically channel-guided porous wood-derived shape-stabilized thermal regulated materials with enhanced thermal conductivity for thermal energy storage. Mater Res Express 2019; 6: 115515.

[38] Cheng F, Zhang X, Wen R, Huang Z, Fang M, Liu Y, et al. Thermal conductivity enhancement of form-

573 stable tetradecanol/expanded perlite composite phase change materials by adding Cu powder and
574 carbon fiber for thermal energy storage. Appl Therm Eng 2019; 156: 653-659.
575 [39] Wang Y, Yu Y, Jing Z, Wang C, Zhou G, Zhao W. Thermal performance of lithium-ion batteries
576 applying forced air cooling with an improved aluminium foam heat sink design. Int J Heat Mass Tran
577 2021; 167: 120827.
578 [40] Li X, Sheng M, Gong S, Wu H, Chen X, Lu X, et al. Flexible and multifunctional phase change
579 composites featuring high-efficiency electromagnetic interference shielding and thermal management
580 for use in electronic devices. Chem Eng J 2022; 430 (Part 2): 132928.
581 [41] Yu Y, Tao Y, Zhao C, Yu X. Thermal storage performance enhancement and regulation mechanism of
582 KNO3-SWCNT based composite phase change materials. Int J Heat Mass Tran 2021; 181: 121870.
583 [42] Zhu C, Chen Y, Cong R, Ran F, Fang G. Improved thermal properties of stearic acid/high density
584 polyethylene/carbon fiber composite heat storage materials. Sol Energ Mat Sol C 2021; 219: 110782.
585 [43] Yang L-Y, Feng C-P, Bai L, Bao R-Y, Liu Z-Y, Yang M-B, et al. Flexible shape-stabilized phase change
586 materials with passive radiative cooling capability for thermal management. Chem Eng J 2021; 425:
587 131466.
588 [44] Li Y, Huang X, Lv J, Wang F, Jiang S, Wang G. Enzymolysis-treated wood-derived hierarchical porous
589 carbon for fluorescence-functionalized phase change materials. Compos Part B-Eng 2022; 234: 109735.
590 [45] Döğüşcü DK, Hekimoğlu G, Sarı A. High internal phase emulsion templated-polystyrene/carbon nano
591 fiber/hexadecanol composites phase change materials for thermal management applications. J Energy
592 Storage 2021; 39: 102674.
593 [46] Zhang Y, Huang J, Cao M, Liu Z, Chen Q. A novel flexible phase change material with well thermal
594 and mechanical properties for lithium batteries application. J Energy Storage 2021; 44 (Part B): 103433.

595 [47] Li W-W, Cheng W-L, Xie B, Liu N, Zhang L-S. Thermal sensitive flexible phase change materials
596 with high thermal conductivity for thermal energy storage. Energ Convers Manage 2017; 149: 1-12.
597 [48] Yang C, Navarro M, Zhao B, Leng G, Xu G, Wang L, et al. Thermal conductivity enhancement of
598 recycled high density polyethylene as a storage media for latent heat thermal energy storage. Sol Energ
599 Mat Sol C 2016; 152: 103-110.
600 [49] Lin X, Zhang X, Ji J, Liu L, Wu Y, Yang M, et al. Development of flexible form-stable phase change
601 material with enhanced electrical resistance for thermal management. J Clean Prod 2021; 311: 127517.
602 [50] Li Z, Wu Y, Zhuang B, Zhao X, Tang Y, Ding X, et al. Preparation of novel copper-powder-sintered
603 frame/paraffin form-stable phase change materials with extremely high thermal conductivity. Appl
604 Energ 2017; 206: 1147-1157.
605 [51] Huang Y-H, Cheng W-L, Zhao R. Thermal management of Li-ion battery pack with the application of
606 flexible form-stable composite phase change materials. Energ Convers Manage 2019; 182: 9-20.
607 [52] Lin X, Zhang X, Ji J, Liu L, Yang M, Zou L. Experimental investigation of form-stable phase change
608 material with enhanced thermal conductivity and thermal-induced flexibility for thermal management.
609 Appl Therm Eng 2022; 201 (Part A): 117762.
610

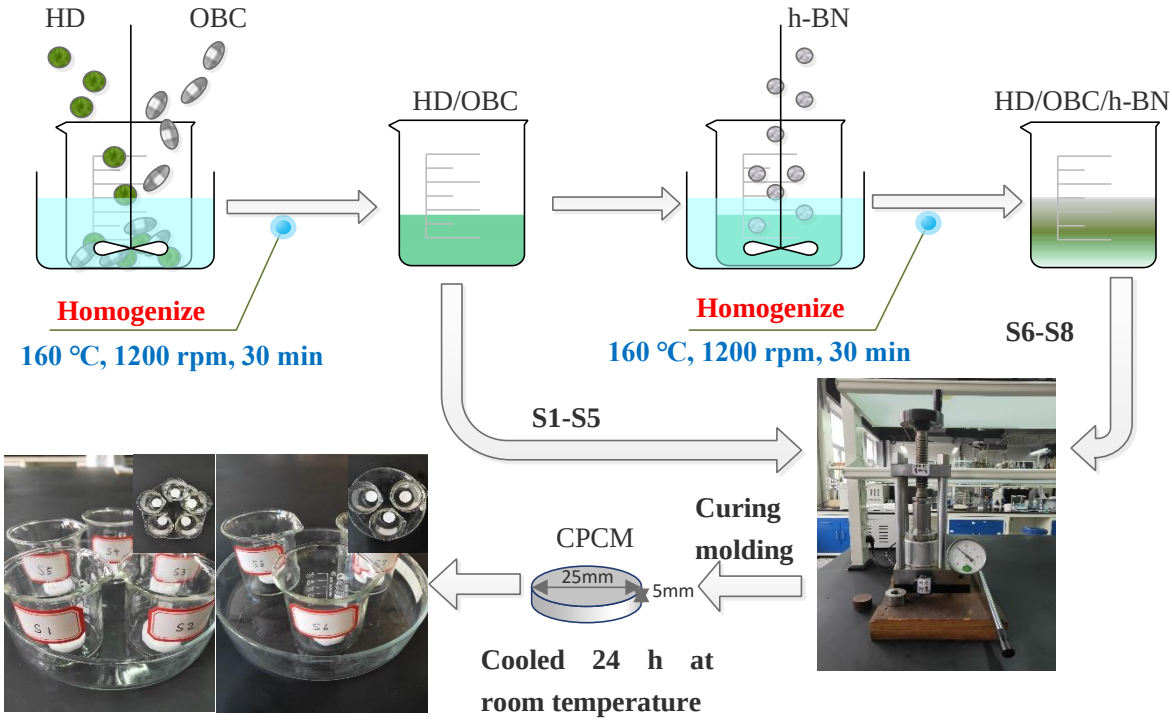

Fig. 1. The preparation process of the CPCMs.

Table 1

The compositions of the HD/OBC/h-BN composites.

Samples	HD (g)	OBC (g)	HD/OBC (mass ratio)	h-BN (g)	Mass fraction of h-BN (%)
S1	18	2	9/1	0	0
S2	16	4	8/2	0	0
S3	14	6	7/3	0	0
S4	12	8	6/4	0	0
S5	10	10	5/5	0	0
S6	11.88	7.92	6/4	0.2	1
S7	11.40	7.60	6/4	1	5
S8	10.80	7.20	6/4	2	10

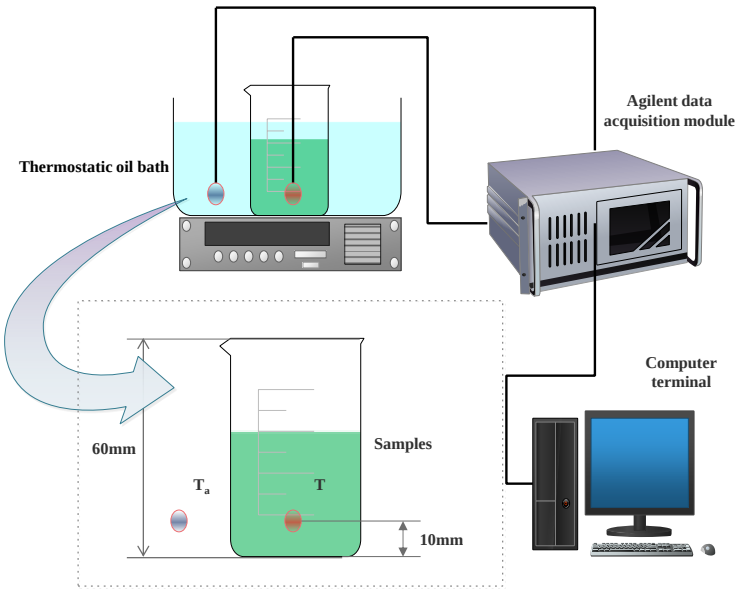

615
616 Fig. 2. Experimental set-up and thermocouple plot of heat storage and release experiment.

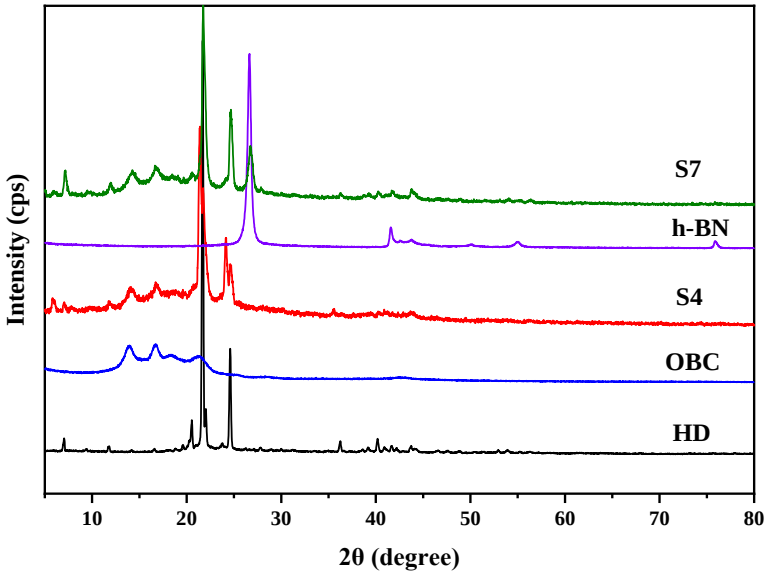

617
618 Fig. 3. XRD experimental results of the HD, OBC, h-BN, HD/OBC (S4) and HD/OBC/h-BN (S7)
619 composite.

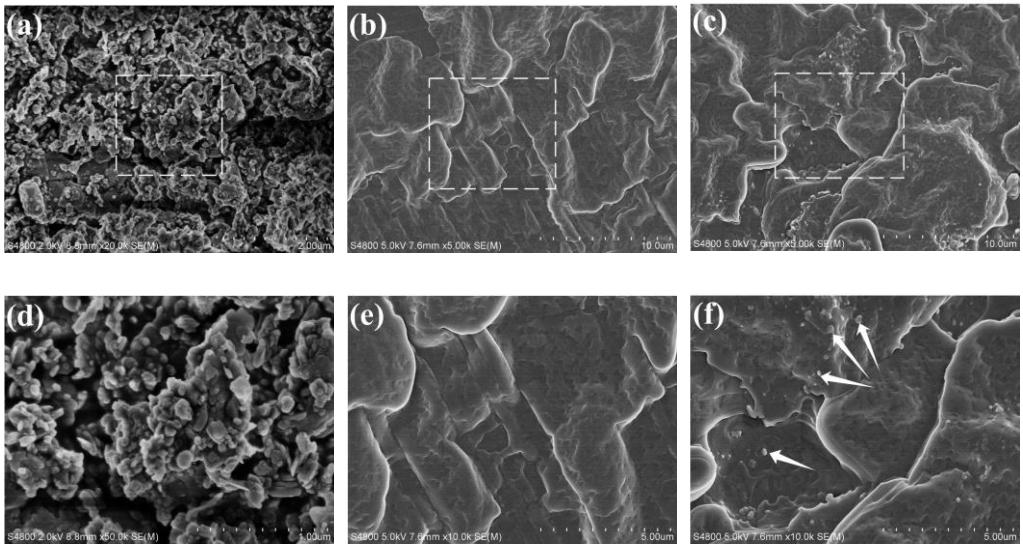

620
621

Fig. 4. Large view morphology structural characterizations of (a) h-BN particles, (b) HD/OBC composite (S4) and (c) HD/OBC/h-BN composite (S7). The dashed line enclosed areas are further studied in high resolution images as (d), (e), and (f) respectively to provide details in h-BN particle distribution in the HD/OBC composite. Evenly distributed h-BN particles are indicated by arrows in figure (f).

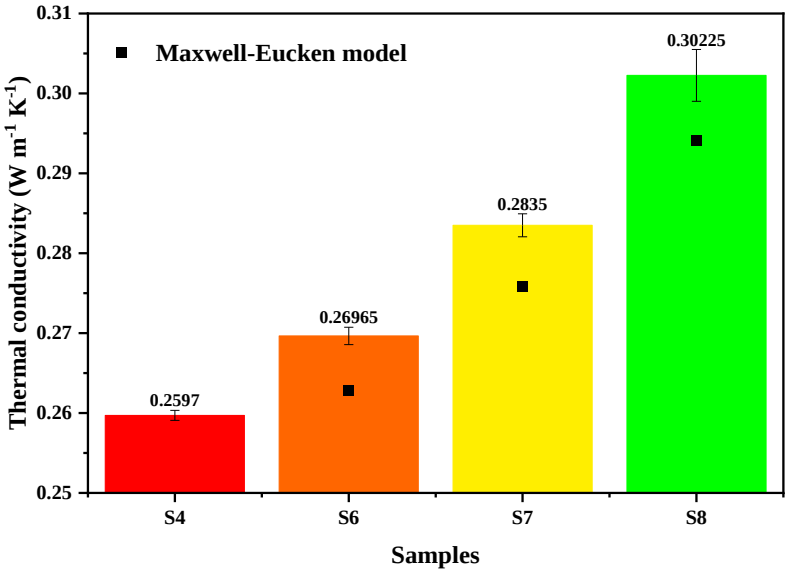

Fig. 5. Thermal conductivity results of the CPCM with different content of h-BN at room temperature.

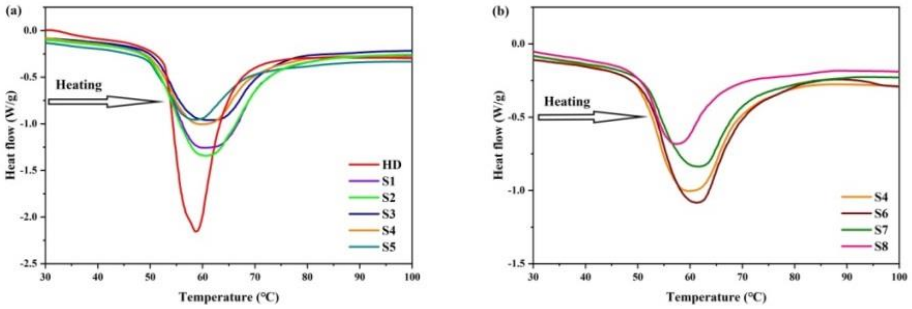

Fig. 6. The phase transition properties of the samples. (a) DSC curves of HD, S1-S5, and (b) S6-S8 at melting process.

Table 2

DSC results of the pure HD and CPCMs.

Samples	T_e (°C)	T_m(°C)	ΔH_m (kJ/g)
HD	52.9	58.7	0.22
S1	50.3	60.4	0.20
S2	50.7	60.6	0.19
S3	50.8	61.5	0.17
S4	50.6	59.6	0.16
S5	49.8	58.5	0.14
S6	51.5	61.2	0.16
S7	53.7	61.6	0.15
S8	50.9	57.4	0.13

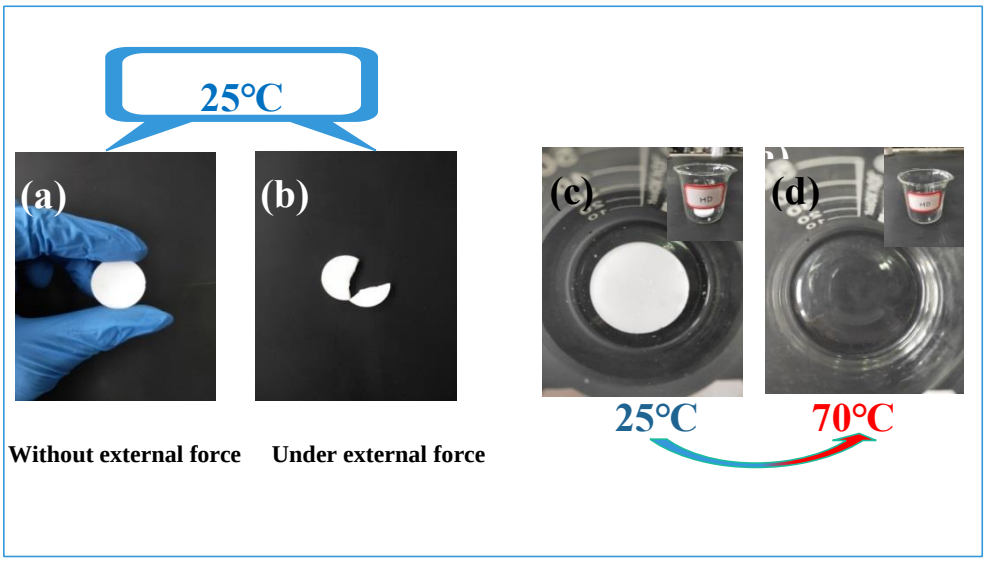

Fig. 7. (a-b)The bending test of pure HD with and without external force at room temperature and (c-d) the leakage of pure HD.

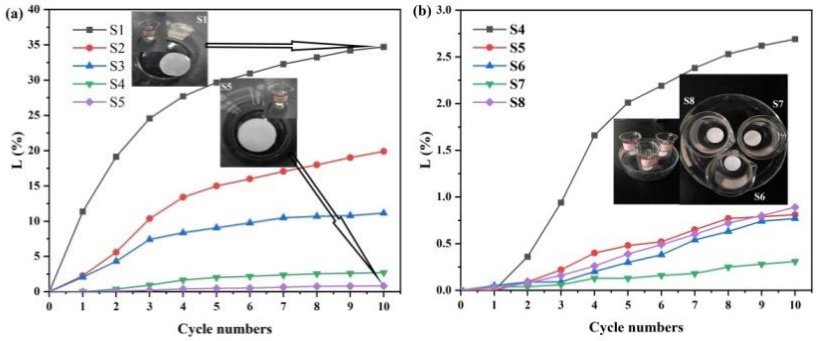

Fig. 8. The leakage rate of different samples (a) S1-S5 and (b) S4-S8 over the test cycle number.

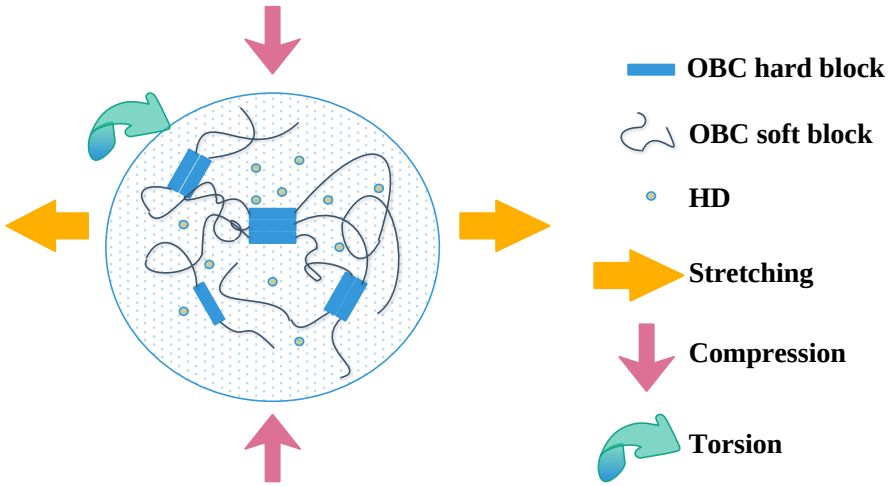

Fig. 9. The basic mechanism diagram of thermally-induced flexible composite with diversity of deformation modes.

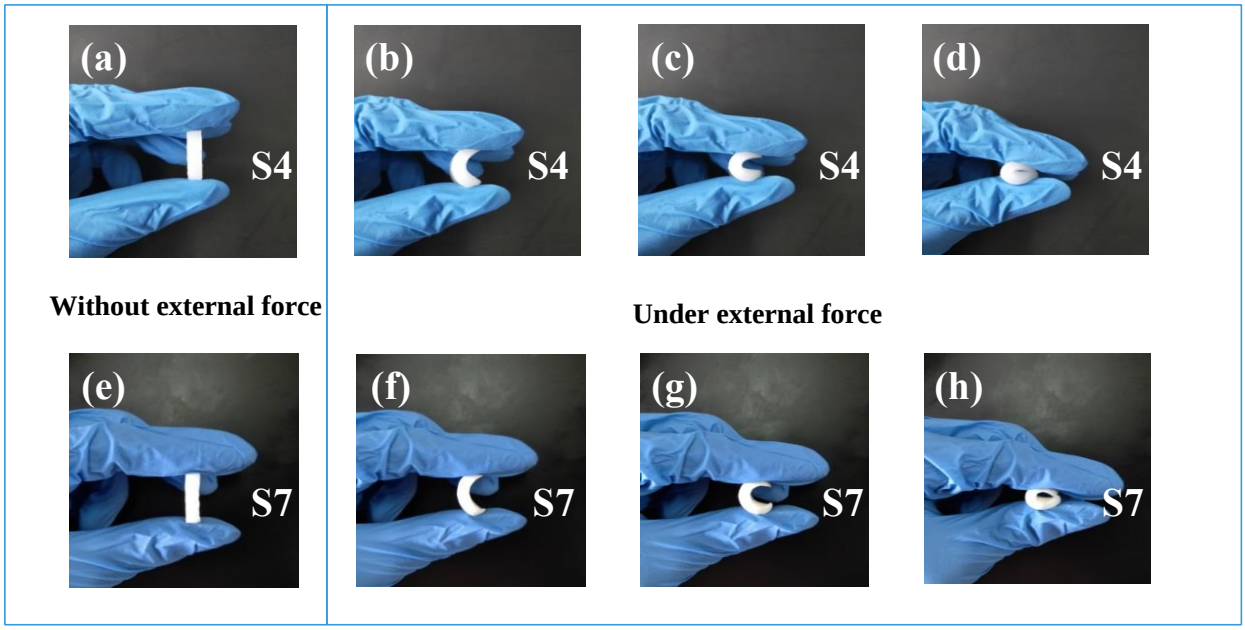

Fig. 10. The bending test of different composites (S4 and S7) with and without external force after heating at 70 °C.

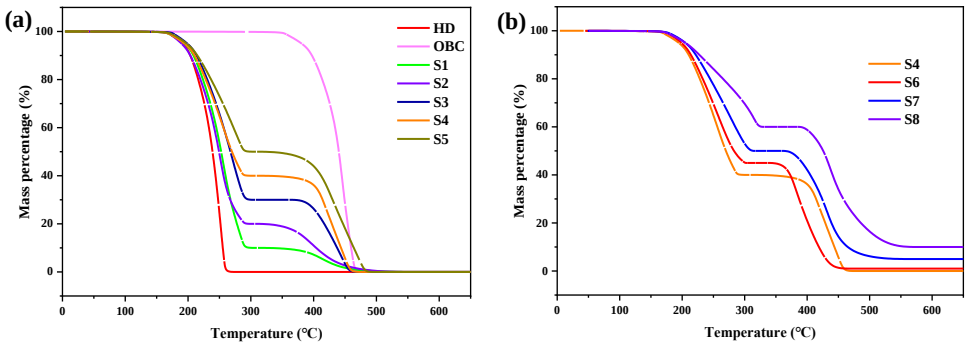

Fig. 11. TGA curves of (a) HD, OBC, S1-S5, (b) S4 and S6-S8.

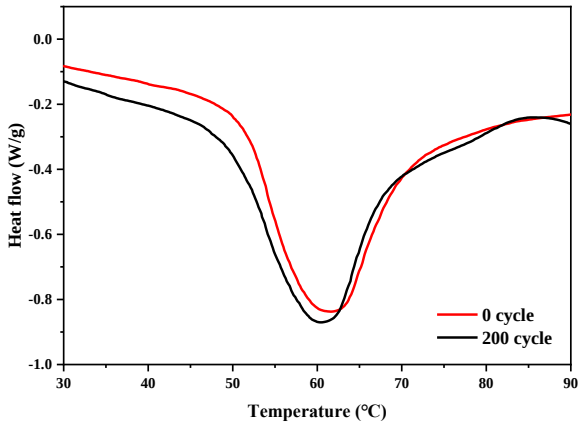

Fig. 12. DSC curves of the S7 before and after 200 thermal cycles.

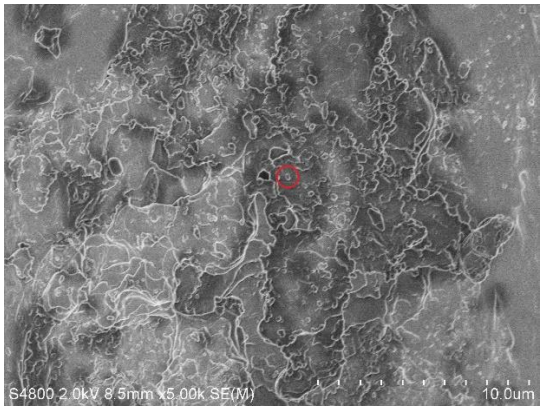

Fig. 13. Morphology structural characterizations of HD/OBC/h-BN composite (S7) after 200 thermal cycles.

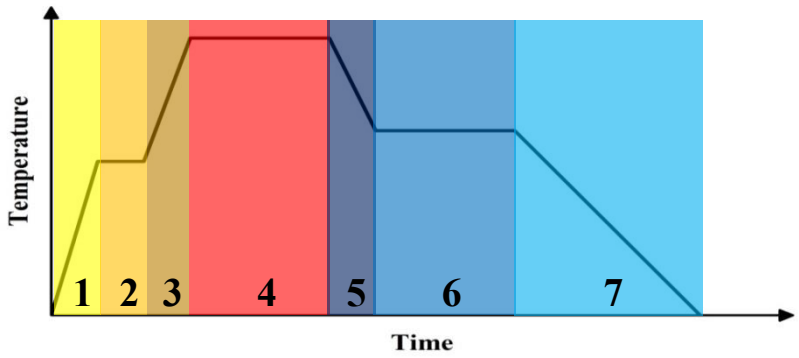

Fig. 14. The ideal temperature curve diagram of heating and cooling processes.

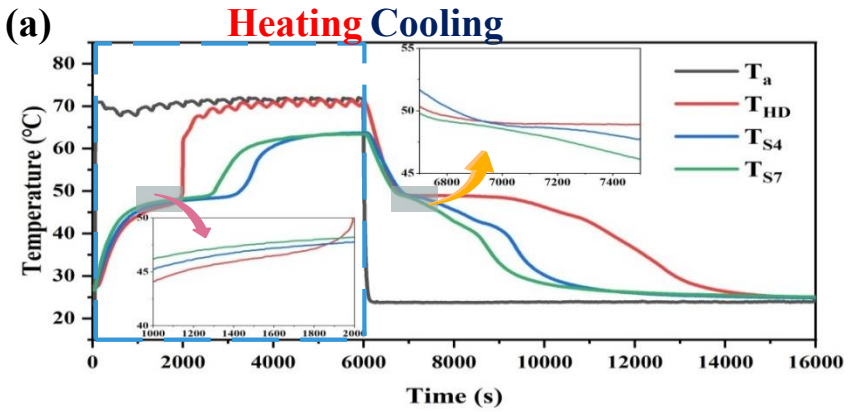

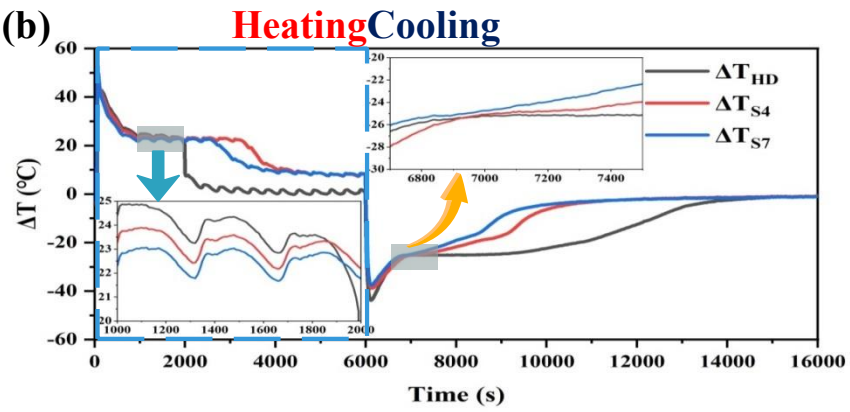

655 Fig. 15. The temperature variation curves of pure HD and different CPCMs during heating and cooling
656 processes: (a) Heat storage and release processes; (b) temperature differences between samples and
657 environment.

658 **Table 3**

659 Time spans of samples in the heating and cooling process.

Samples	Time (s)	
	Phase transition range	
	Heating	Cooling
HD	1150-1990	6730-10340
S4	960-3270	6820-8110
S7	790-2700	6680-7690

660